Inorganic Chemistry

Article

Cite This: Inorg. Chem. XXXX, XXX, XXX-XXX

pubs.acs.org/IC

# Cleavage of Hg−C Bonds of Organomercurials Induced by $Im^{OH}Se$ via Two Distinct Pathways

Mainak Banerjee and Gouriprasanna Roy*

Department of Chemistry, School of Natural Sciences, Shiv Nadar University, NH91, Dadri, Gautam Buddha Nagar, Uttar Pradesh 201314, India

Supporting Information

**ABSTRACT:** We show that the *N*-methylimidazole-based selone $Im^{OH}Se$ having an $N-CH_2CH_2OH$ substituent has the remarkable ability to degrade methylmercury by two distinct pathways. Under basic conditions, $Im^{OH}Se$ converts MeHgCl into biologically inert HgSe nanoparticles and $Me_2Hg$ via the formation of an unstable intermediate $(MeHg)_2Se$ (pathway I). However, under neutral conditions, in the absence of any base, $Im^{OH}Se$ facilitates the cleavage of the Hg−C bond of MeHgCl at room temperature (23 °C), leading to the formation of a stable cleaved product, the tetracoordinated mononuclear mercury compound $(Im^{OH}Se)_2HgCl_2$ and $Me_2Hg$ (pathway II). The initial rate of Hg−C bond cleavage of MeHgCl induced by $Im^{OH}Se$ is almost 2-fold higher than the initial rate observed by $Im^{Me}Se$. Moreover, we show that $Im^{Y}Se$ (Y = OH, Me) has an excellent ability to dealkylate $Me_2Hg$ at room temperature. Under acidic conditions, in the presence of excess $Im^{Y}Se$, the volatile and toxic $Me_2Hg$ further decomposes to the tetracoordinated mononuclear mercury compound $[(Im^{Y}Se)_4Hg]^{2+}$. In addition, the treatment of $Im^{OH}Se$ with MeHgCys or MeHgSG in phosphate buffer (pH 8.5) afforded water-soluble Hg(SeS) nanoparticles via unusual ligand exchange reactions, whereas its derivative $Im^{OMe}Se$ or $Im^{Me}Se$, lacking the $N-CH_2CH_2OH$ substituent, failed to produce Hg(SeS) nanoparticles under identical reaction conditions.

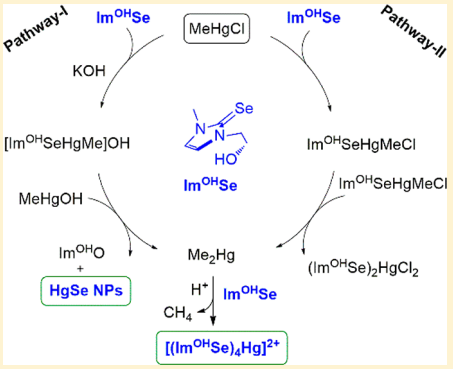


Methylmercury ($MeHg^+$) is considered to be the most toxic form of mercury in the environment due to its ability to accumulate in fat tissues, leading to its biomagnification within the food chain.[1] It can easily cross both the barriers at the blood−brain interface and at the placenta and causes irreversible damage to the central nervous system (CNS) in both adult and developing brains.[2,3] Studies have shown that the nature and extent of mercury toxicity possibly depend on its molecular form.[4−7] In alkaline medium methylmercury may exist in the form of MeHgOH, whereas in acidic medium, under high $Cl^-$ conditions (in human stomach), it may exist in the form of MeHgCl. On the other hand, due to its high affinity for thiol groups, $MeHg^+$ binds with endogenous thiols such as cysteine (CysH) and glutathione (GSH) to form MeHgCys and MeHgSG complexes in the tissues.[8−12] These complexes mainly determine the fate of $MeHg^+$ in the body, and in some cases they facilitate better absorption and uptake of $MeHg^+$ in tissues. For instance, MeHgCys acts as a substrate for L-type large neutral amino acid transporter (LAT1), which actively transports $MeHg^+$ into various tissues, including the brain.[13,14]

It is well-known that the selenium, an important component of many antioxidant enzymes, acts as an antagonist that moderates the toxic effects of both inorganic and organic mercury, including $MeHg^+$ in organisms.[15−18] Its pivotal role in mercury detoxification is based on the strong affinity between mercury and selenium and subsequent formation of organic and inorganic compounds, including biologically inert and less toxic mercury selenide (HgSe) particles.[13,19] HgSe has been found in a wide range of tissues of marine mammals (whales and dolphins)[15,19,20] and also detected in various organs (kidney, liver, muscle, and brain) of humans exposed to $MeHg^+$ species.[21] Reports suggest that the plasma Se-containing protein, selenoprotein P (Sel P), may detoxify heavy metals by sequestering them in the bloodstream.[22] Sel P binds with insoluble $(HgSe)_n$ compounds, formed in the bloodstream of rats by the coadministration of these two elements, and makes them soluble in the form of $\{(Hg-Se)_n\}_m$-Sel P complex.[22d] Additionally, the synthesis of $MeHg^+$-conjugated complexes of selenoamino acids (namely L-selenoglutathione, L-selenocysteine, D,L-selenopenicillamine, and L-selenomethionine),[23] and the cleavage of the Hg−C bond of $MeHg^+$ aided by selenoamino acids,[24] selenoneine,[25−28] and benzimidazole-based selone (1-methyl-1,3-dihydro-2*H*-benzimidazole-2-selone) have been reported in the literature.[29] Recently, we have shown that $Im^{OH}Se$ has the remarkable ability to convert MeHgCl (or MeHgOH), in the presence of 1 equiv of KOH, into insouble HgSe nanoparticles through a facile deselenization process assisted by the neighboring group participation of the −OH group of the $N-CH_2CH_2OH$ substituent of the 1:1 MeHg-conjugated complex $[Im^{OH}SeHgMe]^+$, as illustrated in path A of Figure 1a.[30] The complex $[Im^{OH}SeHgMe]^+$ (15 mM)

Received: May 23, 2017





DOI: 10.1021/acs.inorgchem.7b01301
Inorg. Chem. XXXX, XXX, XXX−XXX

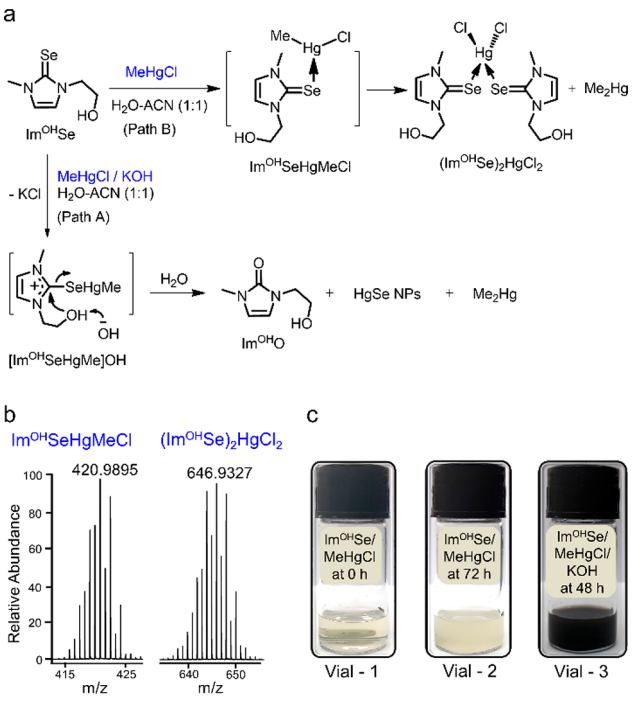


**Figure 1.** (a) Dealkylation of MeHgCl by $Im^{OH}Se$ in the presence (path A) and absence of KOH (path B). (b) Mass spectra of $Im^{OH}SeHgMeCl$ and $(Im^{OH}Se)_2HgCl_2$. (c) Reaction vials showing the formation of a brownish yellow precipitate of $(Im^{OH}Se)_2HgCl_2$ and black HgSe NPs in the reaction of MeHgCl/$Im^{OH}Se$ in the absence and presence of KOH, respectively.

was gradually degraded to near completion in 48 h, in the presence of 1 equiv of KOH, in water/acetonitrile (1/1) at 37 °C (vial 3 in Figure 1c).

However, the treatment of $Im^{OH}Se$ (15 mM) with MeHgCl (15 mM) in water/acetonitrile (1/1) in the absence of KOH did not produce any black precipitate of HgSe nanoparticles in 48 h at 37 °C (under identical reaction conditions). Instead, we isolated a demethylated product, the mononuclear tetracoordinated Hg(II) complex $(Im^{OH}Se)_2HgCl_2$ from the above reaction solution (path B of Figure 1a). Herein we report, for the first time, that $Im^{OH}Se$ has an unique ability to demethylate $MeHg^+$ by two completely different pathways under two different reaction conditions. Detailed studies on the cleavage of Hg−C bonds of various $MeHg^+$ species aided by $Im^{Y}Se$ (Y = OH, OMe, Me) are discussed in this paper.

## RESULTS AND DISCUSSION

The N,N-disubstituted selones $Im^{Y}Se$ (Figure 2) which were used for this study were synthesized by following the literature procedure.[31] When $Im^{OH}Se$ (50 mM) was treated with MeHgCl (1:1 molar ratio) in water/acetonitrile (1/1) solution at room temperature (23 °C), a clear colorless solution was

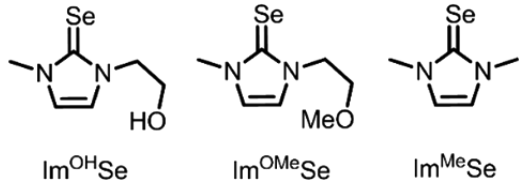


**Figure 2.** Chemical structures of $Im^{Y}Se$ (Y = OH, OMe, Me).

obtained (Figure 1a (path B) and Figure 1c (vial 1)). However, after stirring for 3−4 days at 23 °C, we noticed a gradual formation of a brownish yellow precipitate of the demethylated product $(Im^{OH}Se)_2HgCl_2$ (Figure 1c, vial 2), which was isolated by filtration and characterized thoroughly (yield 53%).

The coordination of $Im^{OH}Se$ to the mercury (Hg) center of MeHgCl was studied in detail by NMR spectroscopy (Figures 3

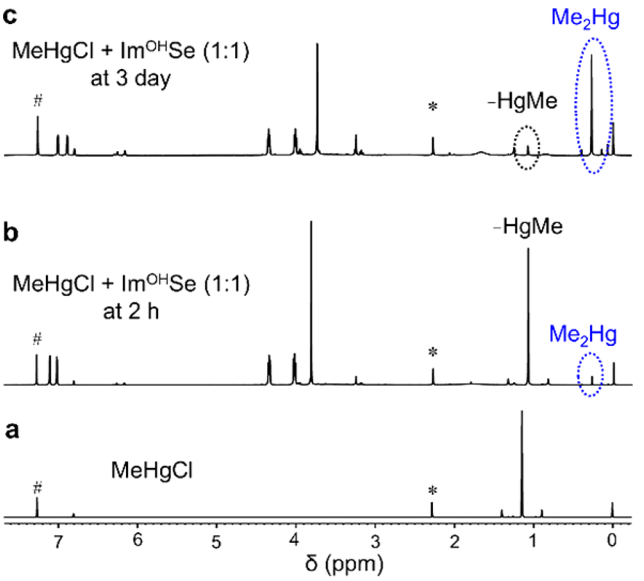


**Figure 3.** $^1H$ NMR spectra showing the cleavage of the Hg−C bond and the formation of $Me_2Hg$ in the reaction of MeHgCl with $Im^{OH}Se$ (1:1 molar ratio) at room temperature (23 °C). Mesitylene was used as external standard. (*, mesitylene peak; #, $CDCl_3$).

and 4). The addition of 1 equiv of $Im^{OH}Se$ (50 mM) into a solution of MeHgCl in $CDCl_3$ (in NMR tube) showed a

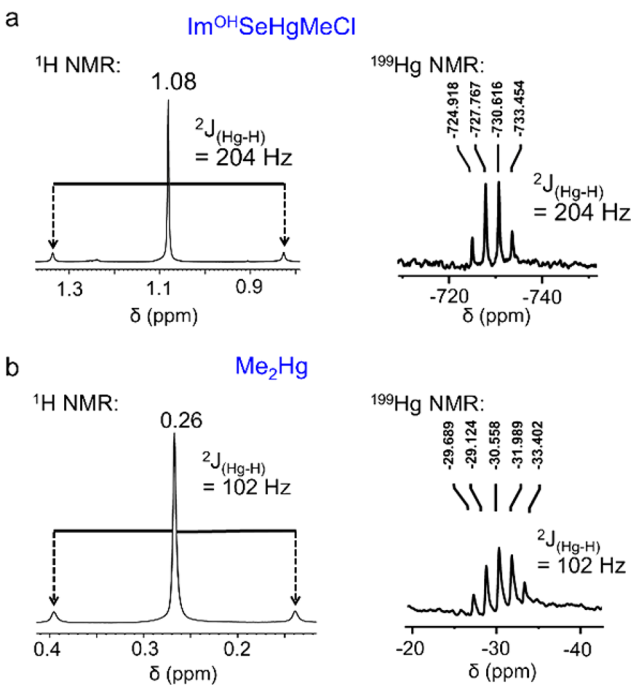


**Figure 4.** $^1H$ (showing only the methyl signal of −HgMe) and $^{199}Hg$ NMR spectra of $Im^{OH}SeHgMeCl$ (a) and $Me_2Hg$ (b) in $CDCl_3$.



DOI: 10.1021/acs.inorgchem.7b01301
Inorg. Chem. XXXX, XXX, XXX−XXX

significant chemical shift in $^{199}$Hg NMR spectroscopy. The $^{199}$Hg NMR signal of the above reaction solution appeared at −730 ppm (Figure 4a), which was shifted almost 78 ppm downfield in comparison to the $^{199}$Hg NMR signal observed for MeHgCl (−808 ppm)(Figure S8 in the Supporting Information), indicating coordination between the Se atom of Im$^{OH}$Se and the Hg center of MeHgCl leading to the formation of the 1:1 adduct Im$^{OH}$SeHgMeCl (Figure 1a, path B).

Similarly, the $^{77}$Se NMR signal of the free ligand Im$^{OH}$Se (−3.8 ppm) has shifted slightly downfield upon addition of 1 equiv of MeHgCl (50 mM). The $^{77}$Se NMR signal of the solution of Im$^{OH}$Se and MeHgCl (1:1 molar ratio) appeared at 7.1 ppm (Figure S3 in the Supporting Information). However, the $^{199}$Hg and $^{77}$Se NMR signals of the cleaved product (Im$^{OH}$Se)$_2$HgCl$_2$ were observed at −1165 and −39 ppm, respectively, in DMSO-$d_6$ (Figure S7 in the Supporting Information, (Im$^{OH}$Se)$_2$HgCl$_2$ is insoluble in chloroform). Although a high-resolution mass spectrometric analysis of the resulting 1:1 adduct Im$^{OH}$SeHgMeCl showed the mass of [Im$^{OH}$SeHgMe]$^+$ ($m/z$ of 420.9895 for [M − Cl]$^+$, Figure 1b), without a chlorine atom; however, due to the strong affinity of Cl$^-$ for mercury, the chlorine atom presumably remained attached to mercury in solution, and thus, it is more appropriate to represent this adduct as Im$^{OH}$SeHgMeCl, rather than [Im$^{OH}$SeHgMe]Cl. The X-ray structure determination of (Im$^{Y}$Se)$_2$HgCl$_2$ has confirmed that the Cl atoms indeed remained attached with Hg(II) (Figure 6). (Im$^{OH}$Se)$_2$HgCl$_2$ showed the $m/z$ 646.9327 (mass of [M − Cl]$^+$, without a chlorine atom) (Figure 1b).

We have calculated the initial rate of cleavage of the Hg−C bond of MeHgCl (initial rate = (2.00 ± 0.1) × 10$^{-3}$ M h$^{-1}$) in the presence of 1 equiv of Im$^{OH}$Se (50 mM) at room temperature (23 °C) (Table 1). $^1$H NMR spectroscopy was used to calculate the initial rate by using mesitylene as external standard (for more details please see the Experimental Section). Significantly, during the progress of the reaction between Im$^{OH}$Se and MeHgCl at room temperature, we observed the gradual disappearance of the methyl signal (1.08 ppm) of −HgCH$_3$ in solution and the concomitant appearance of a new sharp singlet resonance at 0.26 ppm by $^1$H NMR spectroscopy (Figures 3 and 4).

**Table 1. Initial Rates of Cleavage of Hg−C Bonds of MeHgCl or EtHgCl Induced by Im$^{Y}$Se**

| | initial rate (10$^{-3}$ M h$^{-1}$)[a] | |
|---|---|---|
| compd | Me−Hg bond | Et−Hg bond |
| Im$^{OH}$Se | 2.00 ± 0.1 | 1.50 ± 0.16 |
| Im$^{OMe}$Se | 1.47 ± 0.29 | 0.98 ± 0.11 |
| Im$^{Me}$Se | 0.84 ± 0.07 | 0.64 ± 0.13 |

[a]All experiments were carried out at least three times in an NMR tube at room temperature (23 °C) in CDCl$_3$ ([RHgX]/[Im$^{Y}$Se] = 1; [RHgX] = 50 mM; R = Me, Et; see the Experimental Section).

The $^{199}$Hg NMR studies have confirmed the formation of dimethylmercury (Me$_2$Hg) as a new product (Figure 4b) in the reaction solution. The $^{199}$Hg NMR (proton-coupled) signal of Me$_2$Hg was observed as a heptet at −30.5 ppm in CDCl$_3$ (−113 ppm in DMSO-$d_6$).[32] The $^2J$($^{199}$Hg−$^1$H) coupling constant values for the 1:1 adduct Im$^{OH}$SeHgMeCl and Me$_2$Hg were 204 and 102 Hz, respectively (Figure 4), indicating that $^2J$($^{199}$Hg−$^1$H) coupling constant values are influenced by the nature of the X group of MeHgX. In addition, $^1$H NMR studies in polar aprotic solvent (DMSO-$d_6$) have revealed that the −OH group of the N−CH$_2$CH$_2$OH substituent of Im$^{OH}$Se did not participate in coordination to the mercury center and it remained free in the reaction solution of Im$^{OH}$Se and MeHgCl (1:1 molar ratio), and in the isolated cleaved product (Im$^{OH}$Se)$_2$HgCl$_2$ (Figures S1, S4, and S6 in the Supporting Information).

Moreover, to know whether there is any role of N substitution of Im$^{OH}$Se in the cleavage of the Hg−C bond, we have employed two other derivatives of Im$^{OH}$Se (Im$^{OMe}$Se and Im$^{Me}$Se) in our study (Figure 2). Like Im$^{OH}$Se, the treatment of Im$^{Y}$Se (50 mM, Y = OMe, Me) with MeHgCl (1:1 molar ratio) in water/acetonitrile (1/1) solution, in the absence of KOH, afforded stable tetracoordinated Hg(II) complexes (Im$^{Y}$Se)$_2$HgCl$_2$ and Me$_2$Hg (Scheme 1). The initial rate of Hg−C bond cleavage of MeHgCl by Im$^{OMe}$Se is (1.47 ± 0.29) × 10$^{-3}$ M h$^{-1}$, which is slightly slower than the initial rate of Hg−C bond cleavage of MeHgCl by Im$^{OH}$Se (Table 1). On the other hand, the initial rate of Hg−C bond cleavage of MeHgCl by Im$^{Me}$Se ((0.84 ± 0.07) × 10$^{-3}$ M h$^{-1}$) is almost 2-fold slower than the initial rate obtained by Im$^{OH}$Se (Figure 5 and Table 1).

**Scheme 1. Synthetic Scheme for the Formation of (Im$^{Y}$Se)$_2$HgCl$_2$**

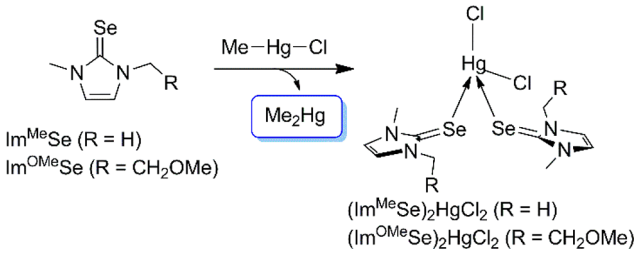


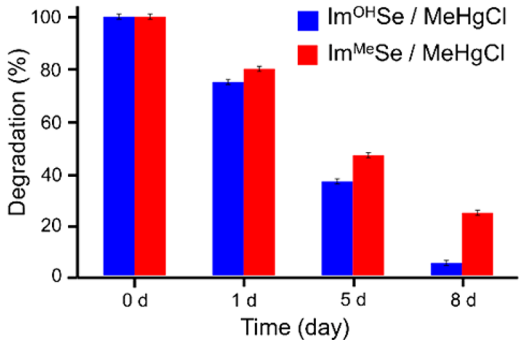


**Figure 5.** Bar diagram showing the degradation of MeHgCl induced by Im$^{Y}$Se (Y = OH, Me) over time. The reactions were monitored by $^1$H NMR spectroscopy by following the cleavage of Hg−C bonds at room temperature (23 °C).

From X-ray crystal structures and quantum mechanical calculations (DFT), it is evident that these three imidazole-based selones (Im$^{OH}$Se, Im$^{Me}$Se, and Im$^{OMe}$Se) mainly exist in zwitterionic form with a negative charge on the Se atoms and a delocalized positive charge on the imidazole ring (Table 2 and Figure S40 in the Supporting Information). The higher reactivity of Im$^{OH}$Se in comparison to the two other derivatives is probably due to the presence of a more negative charge on the Se atom of Im$^{OH}$Se (−0.32 au) in comparison to that in


DOI: 10.1021/acs.inorgchem.7b01301
Inorg. Chem. XXXX, XXX, XXX−XXX

**Table 2. C−Se Bond Lengths, Bond Orders, and Charges on Se Atoms of $Im^{Y}Se$**

| compd | C−Se bond length (Å) (calcd) | C−Se bond order (calcd)[a] | charge on Se (au)[a] |
|---|---|---|---|
| $Im^{OH}Se$ | 1.856 | 1.274 | −0.316 |
| $Im^{OMe}Se$ | 1.843 | 1.340 | −0.286 |
| $Im^{Me}Se$ | 1.837 | 1.356 | −0.271 |

[a]Optimization and natural bond orbital (NBO) analysis was performed at the B3LYP/6-311++G(2d,p) level of theory (details are mentioned in the Experimental Section).

$Im^{OMe}Se$ (−0.29 au) or $Im^{Me}Se$ (−0.27 au) (Table 2). This could possibly lead to the formation of a strong bond between the Se atom of $Im^{OH}Se$ and the Hg atom of MeHgCl, which may eventually help in the weakening, and hence facile cleavage, of the Hg−$CH_3$ bond. The higher negative charge on the Se atom of $Im^{OH}Se$ is probably due to the presence of hydrogen bonding between the Se atom of one molecular unit with the OH group of other molecular unit as shown in the crystal structure, leading to the formation of a chainlike structure (Figure S44 in the Supporting Information). Consequently, because of this H bonding, the C−Se bond length of $Im^{OH}Se$ has increased substantially in comparison to the C−Se bond lengths of $Im^{Me}Se$ and $Im^{OMe}Se$ (Table 2).

The tetracoordinated mercury complexes $(Im^{OMe}Se)_2HgCl_2$ (yield 37%) and $(Im^{Me}Se)_2HgCl_2$ (yield 29%) were isolated from the respective reaction solutions and characterized thoroughly. The single-crystal X-ray analyses of $(Im^{OMe}Se)_2HgCl_2$ ($\tau$ = 0.96)[33] and $(Im^{Me}Se)_2HgCl_2$ ($\tau$ = 1.02) have confirmed the tetrahedral geometry at the mercury center of both complexes (Figure 6). The two Hg−Cl and Hg−Se bonds in $(Im^{OMe}Se)_2HgCl_2$ are equal in length (Hg−Cl1 = Hg−Cl2 = 2.526 Å; Hg−Se1 = Hg−Se1′ = 2.609 Å). The C−Se bond length in $(Im^{OMe}Se)_2HgCl_2$ is significantly longer (C2−Se1 = C2′−Se1′ = 1.868 Å) in comparison to that in the free ligand $Im^{OMe}Se$ (C2−Se = 1.837 Å (Experimental) Table S5 in the Supporting Information), indicating a quite strong interaction between Se and Hg(II) atoms in the complex $(Im^{OMe}Se)_2HgCl_2$ (Tables S2 and S3 in the Supporting Information). Moreover, because of the coordination to the mercury center through the p-type lone pair of the Se atom of $Im^{Y}Se$, the zwitterionic character of the mercury-bound $Im^{Y}Se$ in tetracoordinated Hg(II) complexes $(Im^{Y}Se)_2HgCl_2$ is increased substantially in comparison to that in free $Im^{Y}Se$ (Figures S41−S43 in the Supporting Information).[34] The overall positive charge on the imidazole ring of bound $Im^{Y}Se$ of $(Im^{Y}Se)_2HgCl_2$ has also increased significantly in comparison to that in free $Im^{Y}Se$. As a consequence of the coordination to the mercury center, the $^1H$ NMR spectra of $(Im^{Y}Se)_2HgCl_2$ showed a significant downfield shift of the proton resonance of bound $Im^{Y}Se$ in comparison to the proton resonance of free $Im^{Y}Se$ (Figures S15−S17 in the Supporting Information).

Crystal-packing arrangements of $(Im^{OMe}Se)_2HgCl_2$ in the solid state show the presence of nonbonded intermolecular C−H···Cl hydrogen-bonding interactions in $(Im^{OMe}Se)_2HgCl_2$. Two Cl atoms of one molecular unit are forming strong intermolecular C−H···Cl hydrogen bonding ($d_{CH\cdots Cl}$ = 2.689 Å) with the olefinic H atom (or (imidazole)CH) of two different molecular units on either side of the molecule leading to the formation of a zigzag-like network, as shown in Figure 7a. In addition to that, strong nonbonded intermolecular C−H···O hydrogen-bonding ($d_{CH\cdots O}$ = 2.517 Å) interactions are also present between the two molecular units in the solid-state crystal structure, as illustrated in Figure 7b. On the other hand, in the case of $(Im^{Me}Se)_2HgCl_2$, the H atom of the −NMe group

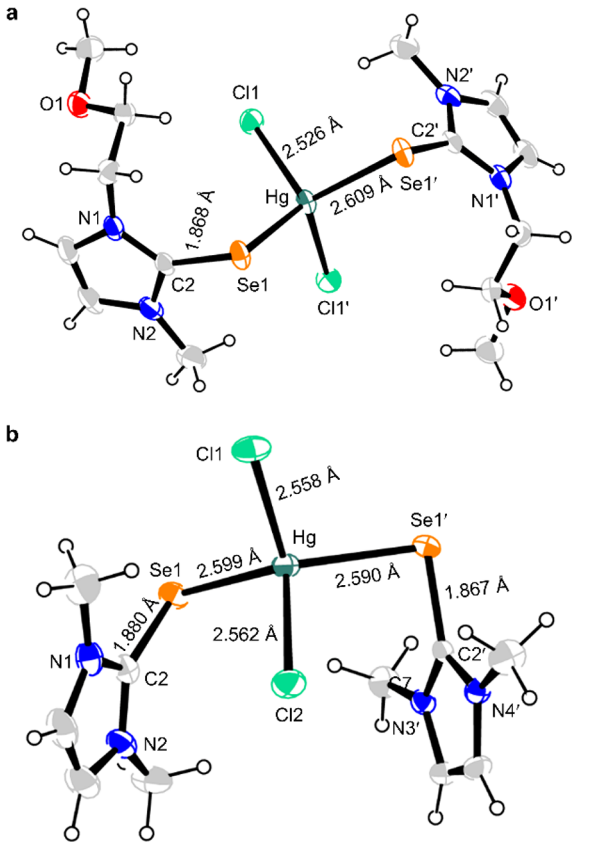


**Figure 6.** ORTEP images of (a) $(Im^{OMe}Se)_2HgCl_2$ and (b) $(Im^{Me}Se)_2HgCl_2$.

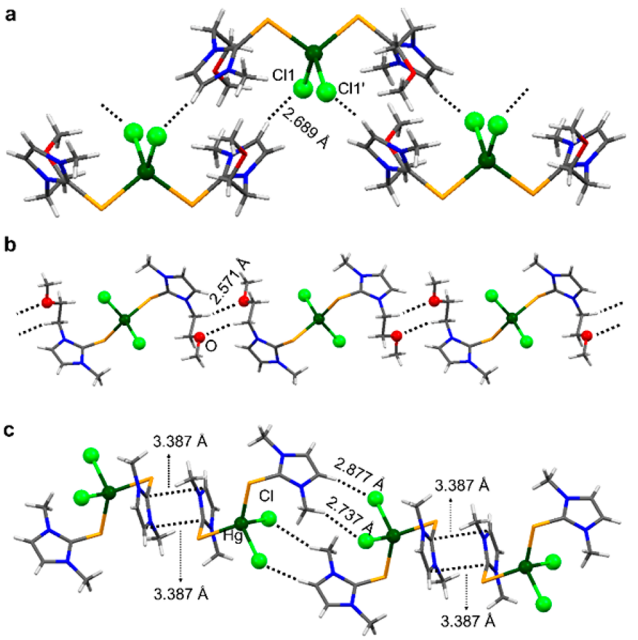


**Figure 7.** Crystal packing of $(Im^{OMe}Se)_2HgCl_2$ showing intermolecular C−H···Cl (a) and C−H···Cl (b) hydrogen bonding interactions. (c) Crystal packing of $(Im^{Me}Se)_2HgCl_2$ showing intermolecular C−H···Cl hydrogen bonding and the $\pi$−$\pi$ interaction between two imidazole rings.



DOI: 10.1021/acs.inorgchem.7b01301
Inorg. Chem. XXXX, XXX, XXX−XXX

and the olefinic H atom of one molecular unit are forming distinct nonbonded intermolecular C−H···Cl hydrogen-bonding interactions with the Cl atoms of other molecular unit ($d_{ImCH\cdots Cl}$ = 2.877 Å; $d_{(NMe)H\cdots Cl}$ = 2.737 Å), leading to the formation of a dimeric structure (Figure 7c). In addition to that, the presence of a distinct $\pi-\pi$ interaction between the two imidazole rings of two different molecular units of $(Im^{Me}Se)_2HgCl_2$ is observed in the crystal-packing geometry. The $\pi-\pi$ interfacial distance between the two imidazole rings in the crystal lattice is 3.387 Å, as shown in Figure 7c.[35]

In order to investigate the effect of $Im^YSe$ on the cleavage of Hg−C bonds of other organomercurials, we have employed ethylmercury chloride (EtHgCl) in our study. The treatment of $Im^YSe$ (50 mM; Y = OH, Me, OMe) with EtHgCl (1:1 molar ratio) in water/acetonitrile (1/1) solution at room temperature yielded the 1:1 adduct $Im^YSeHgEtCl$. However, we noticed the gradual cleavage of Hg−C bonds of $Im^YSeHgEtCl$ and the formation of stable Hg(II) complexes $[(Im^YSe)_2HgCl_2]$ and diethylmercury ($Et_2Hg$).[36] The cleavage of the Hg−C bond of EtHgCl aided by $Im^YSe$ was followed by NMR spectroscopy (Figures 8 and 9 and Figure S19 in the Supporting

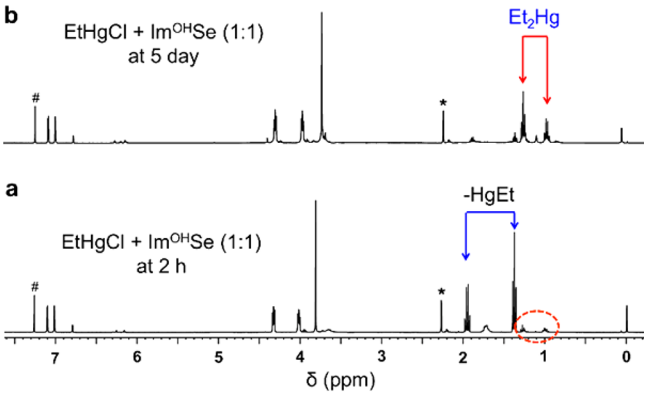


**Figure 8.** $^1H$ NMR spectra, in $CDCl_3$, showing the cleavage of the Hg−C bond of EtHgCl and the formation of $Et_2Hg$ in the reaction of EtHgCl/$Im^{OH}Se$ (1:1 molar ratio) at 23 °C. Mesitylene was used as an external standard (*, mesitylene peak; #, $CDCl_3$).

Information). The $^{199}Hg$ NMR (proton-coupled) signal of $Et_2Hg$ was observed at −328.5 ppm in $CDCl_3$ (Figure 9b). The $^2J(^{199}Hg-^1H)$ and $^3J(^{199}Hg-^1H)$ coupling constant values for $Et_2Hg$ were 96.8 and 126.6 Hz, respectively. The $^2J(^{199}Hg-^1H)$ and $^3J(^{199}Hg-^1H)$ coupling constant values for the 1:1 adduct $Im^{OH}SeHgEtCl$ were 199 and 299.2 Hz, respectively (Figure 9a). Significantly, the initial rates of the Hg−Et bond cleavage by $Im^YSe$ were found to be slightly slower than the initial rates of cleavage of the Hg−Me bond by $Im^YSe$ under identical reaction conditions (Table 1).

The formation of highly toxic volatile $Me_2Hg$ in the reaction of MeHgCl and $Im^YSe$ (1:1 molar ratio) is a serious concern considering the usefulness of these imidazole-based selones in the context of detoxification of neurotoxic methylmercury. Khan and co-workers have studied the demethylation of methylmercury by several selenoamino acids, including naturally occurring L-selenocysteine (one of the components of several seleno-enzymes including selenoprotein P, glutathione peroxidase, and thioredoxin reductase), where they have reported the conversion of toxic methylmercury to the unstable intermediate bis(methylmercuric)selenide $(MeHg)_2Se$ (half-life ~1 h), which was readily degraded to biologically inert HgSe(s)

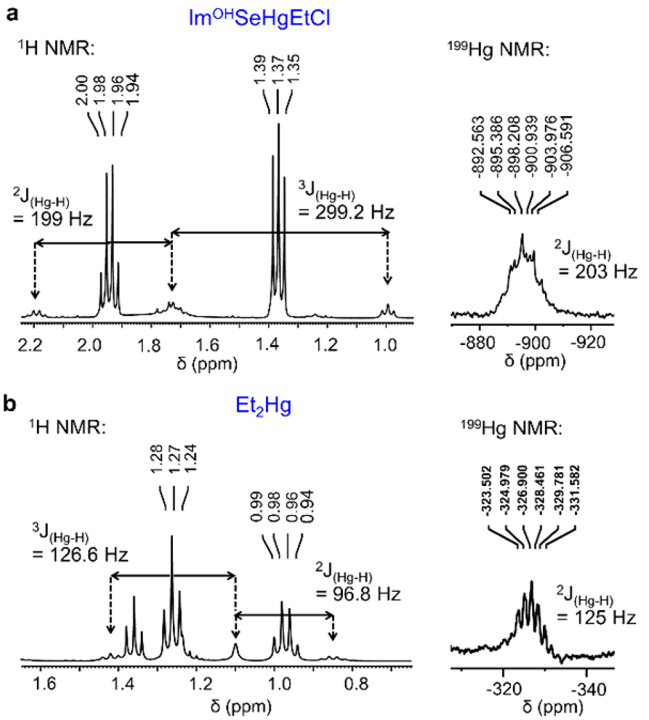


**Figure 9.** $^1H$ (showing only the ethyl peak of −HgEt group) and $^{199}Hg$ NMR spectra of $Im^{OH}SeHgEtCl$ (a) and $Et_2Hg$ (b) in $CDCl_3$.

and $Me_2Hg$.[24] In nature, the conversion of methylmercury to $Me_2Hg$ in the presence of $H_2S$ has also been reported in the literature.[37,38] Moreover, Baldi and co-workers have reported that the sulfate-reducing bacteria (two different axenic cultures of strains of the mercury resistance sulfate-reducing bacterium *Desulfovibrio desulfuricans*) showed mercury tolerance by converting toxic methylmercury to less toxic insoluble HgS(s) and $Me_2Hg$ via the formation of unstable intermediate $(MeHg)_2S$.[39−41] The volatile hydrocarbon $CH_4$ was detected in the *D. desulfuricans* cultures spiked with MeHgCl, and the possible pathway of formation of $CH_4$ was due to the degradation of $Me_2Hg$ under the acidic conditions (pH 6.3) of cultures.[39] Several reports suggest that $Me_2Hg$ may decompose slowly into methylmercury and $CH_4$ under acidic conditions (Scheme 2).[39,42] Furthermore, the protolytic

**Scheme 2. Decomposition of $Me_2Hg$ in the Absence and Presence of Excess $Im^YSe$, under Acidic Conditions**

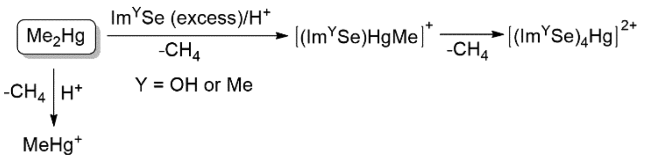


cleavage of the Hg−C bond of methylmercury induced by *N*-methyl-substituted benzimidazole-based selone (1-methyl-1,3-dihydro-2*H*-benzimidazole-2-selone) and subsequently the liberation of $CH_4$ has been reported by Parkin et al.[29] The report suggests that $Me_2Hg$ is notoriously inert toward cleavage of the Hg−C bond under physiological conditions, and it reacts very slowly with biologically relevant dithiol, dihydrolipoic acid derivative, at 37 °C to cleave one of the Hg−$CH_3$ bonds; however, cleavage of the second Hg−$CH_3$ bond could not be achieved.[43]


DOI: 10.1021/acs.inorgchem.7b01301
Inorg. Chem. XXXX, XXX, XXX−XXX

We have studied the demethylation of $Me_2Hg$ in the presence or absence of nucleophilic selenium compounds $Im^YSe$ ($[Im^YSe]/[Me_2Hg] = 4$; Y = OH, Me) under acidic conditions (in the presence of 1 equiv of formic acid or tetrafluoroboric acid) by $^1H$ NMR spectroscopy. The rate of Hg−C bond cleavage of $Me_2Hg$ was found to be almost 2-fold faster in the presence of $Im^{OH}Se$ (Figure 10). The initial rates

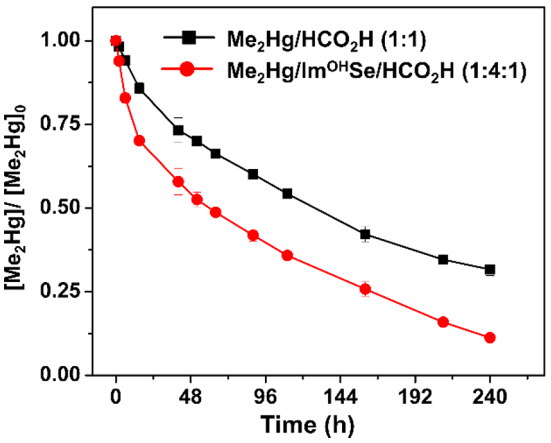


**Figure 10.** Demethylation of $Me_2Hg$ under acidic conditions in the presence and absence of $Im^{OH}Se$ (for more details see the Experimental Section).

of cleavage of the Hg−$CH_3$ bond of $Me_2Hg$ in the presence and absence of $Im^{OH}Se$ are $(14.1 \pm 0.01) \times 10^{-4}$ and $(7.5 \pm 0.01) \times 10^{-4}$ M $h^{-1}$, respectively. Under acidic conditions, $Me_2Hg$ was degraded to $MeHg^+$ and $CH_4$ (Scheme 2 and Figures S20 and S21 in the Supporting Information). However, during the decomposition of $Me_2Hg$ in the presence of excess $Im^YSe$ (Y = OH, Me), we did not observe the formation of significant amounts of $MeHg^+$ from $Me_2Hg$, indicating that the $MeHg^+$, produced during the decomposition of $Me_2Hg$, further reacted with $Im^YSe$ (excess) to form the tetracoordinated Hg(II) complex $[(Im^YSe)_4Hg]^{2+}$. The near-completion of degradation of $Me_2Hg$ (50 mM) was observed in the presence of excess $Im^YSe$ (1:4 molar ratio) under acidic conditions. Nice cubic-shaped colorless crystals of $[(Im^{Me}Se)_4Hg](BF_4)_2$ were isolated from the reaction solution of $Me_2Hg/Im^{Me}Se/HBF_4$ (1:4:1 molar ratio) in DMSO-$d_6$ in an NMR tube after long standing (Figure 11 and the Experimental Section). The single-crystal X-ray structure analysis of $[(Im^{Me}Se)_4Hg](BF_4)_2$ showed that all four Se atoms of $Im^{Me}Se$ are coordinated to the same Hg(II) atom in an unsymmetrical manner, as illustrated in Figure 11. The Hg−Se bond lengths in $[(Im^{Me}Se)_4Hg](BF_4)_2$ are comparable to the mean value of 2.643 Å for compounds listed in the Cambridge Structural Database.[29,44] The Se2 and Se4 atoms are coordinated strongly to the tetrahedral Hg(II) center ($d_{Hg-Se2}$ = 2.618 Å, $d_{Hg-Se4}$ = 2.607 Å), whereas the other two selenium atoms, Se1 and Se4, are coordinated relatively weakly to the same Hg(II) center ($d_{Hg-Se1}$ = 2.660 Å, $d_{Hg-Se3}$ = 2.639 Å). Crystal-packing arrangements of $[(Im^{Me}Se)_4Hg](BF_4)_2$ in the solid state showed the presence of multiple nonbonded intermolecular C−H···F hydrogen-bonding interactions (Figure S23 in the Supporting Information). Selected bond lengths and bond angles are given in Table S4 in the Supporting Information.

On the basis of our experimental observations we found that the nature of the final product in the reaction of $Im^{OH}Se$ and

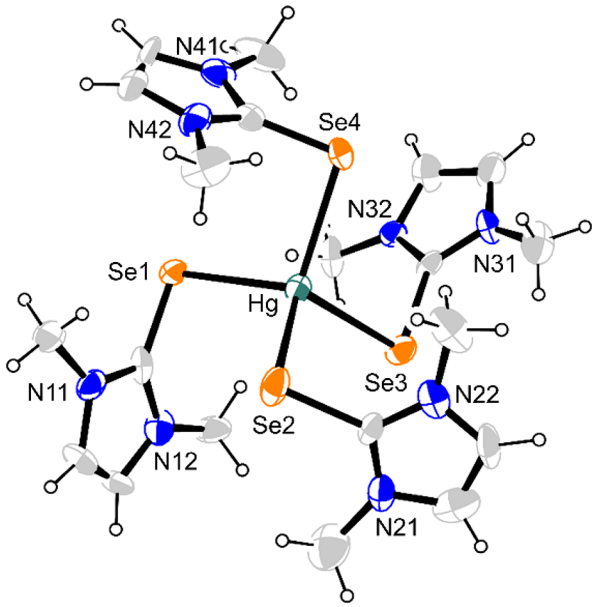


**Figure 11.** Molecular structure of the cation $[(Im^{Me}Se)_4Hg]^{2+}$ of $[(Im^{Me}Se)_4Hg](BF_4)_2$. Two $BF_4^-$ anions are removed for clarity.

MeHgCl is completely dependent upon the reaction conditions. Under basic conditions, the treatment of MeHgCl with $Im^{OH}Se$ afforded the highly unstable 1:1 MeHg-conjugated complex $[Im^{OH}SeHgMeHg]OH$, which was readily degraded into $Im^{OH}O$ and $(MeHg)_2Se$. The unstable $(MeHg)_2Se$ was further decomposed into insoluble HgSe(s) nanoparticles and $Me_2Hg$, as shown in pathway I in Scheme 3a.[30a] The ketone $Im^{OH}O$ was formed in the reaction via the formation of the positively charged cyclic intermediate I (Scheme 3b,c). DFT calculations showed that the nucleophilic attack at the C1 center of the unstable intermediate I was thermodynamically more favorable (35.7 kcal/mol, path A) over the nucleophilic attack at the C2 center (path B) (Figure S46 in the Supporting Information). The C1−O bond length is 1.487 Å, which is much longer (and weaker) than the C2−O bond length (1.312 Å), and thus, the formation of ketone $Im^{OH}O$ through path A is possibly the favorable pathway (Scheme 3c). On the other hand, the reactions of MeHgCl with $Im^{OH}Se$, in the absence of KOH (under neutral conditions), yielded the 1:1 adduct $Im^{OH}SeHgMeCl$ at room temperature. However, in the presence of the electron-donating ligand $Im^{OH}Se$, facile cleavage of the Hg−$CH_3$ bond was observed, leading to the formation of $Me_2Hg$ and stable tetracoordinated mononuclear mercury complex $(Im^{OH}Se)_2HgCl_2$ via the possible four-membered cyclic intermediate II, as mentioned in Scheme 3a (pathway II) and Scheme 3c. The exchange of R and X atoms between the Hg−R/Hg−X groups through a four-membered cyclic intermediate has been reported in the literature.[45]

It is well-known that methylmercury binds with endogenous thiols, including cysteine and glutathione, in tissues.[8] Studies have shown that hemoglobin (Hb) is a major methylmercury binding protein in the blood of marine mammals (dolphin) and the cysteine residue on the dolphin Hb $\beta$-chain is found to be the main binding site.[46] The cysteine-conjugated methylmercury complex MeHgCys is known to facilitate methylmercury uptake into various tissues. For instance, mice treated with MeHgCys had approximately 50% and 250% increased uptake of mercury in brain and liver, respectively, in comparison with mice treated with MeHgCl.[8] On the other hand, methyl-


DOI: 10.1021/acs.inorgchem.7b01301
Inorg. Chem. XXXX, XXX, XXX−XXX

**Scheme 3. Proposed Pathways of Degradation of MeHgCl by $Im^{OH}Se$**

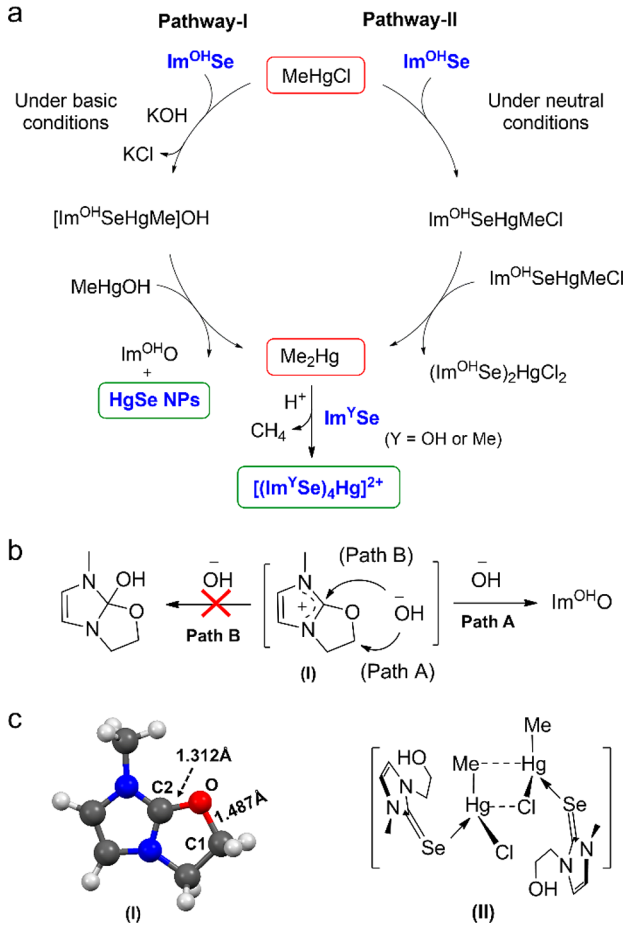


mercury is known to decrease the intracellular GSH content by forming the glutathione-conjugated methylmercury complex MeHgSG, and thereby it increases the production of reactive oxygen species (ROS) in various tissues leading to DNA damage, protein oxidation, lipid peroxidation, and cell death.[15,47] Therefore, as part of this current study, we have also investigated the ability of $Im^{OH}Se$ to degrade other methylmercury species such as MeHgCys and MeHgSG.

When MeHgCys (30 mM, $m/z$ 338.0142) was treated with $Im^{OH}Se$ in a 1:1 molar ratio in phosphate buffer (pH 8.5), the nearly colorless solution turned gray to blackish gray over the time as the reaction was allowed to proceed at 37 °C (Figure 12a, reaction vials). Aliquots of the above reaction solution were collected at various time intervals to monitor the reaction by HPLC (Figure S29 in the Supporting Information). HPLC studies showed that the peak area corresponding to the MeHg-conjugated complex $[Im^{OH}SeHgMe]Cys$ ($m/z$ 420.9915) at a retention time of 10.95 min decreased gradually, indicating that the complex $[Im^{OH}SeHgMe]Cys$ was unstable at pH 8.5. After near-completion of the reaction in 72 h we isolated the blackish gray HgSe nanoparticles by centrifugation. The corresponding ketone $Im^{OH}O$ (at a retention time of 7.01 min in the HPLC chromatogram) was isolated (yield 27%) from the supernatant and characterized thoroughly. The $^{199}Hg$ NMR with a peak at −113 ppm in DMSO-$d_6$ confirmed the formation of $Me_2Hg$ in the reaction solution (Figure S34 in the Supporting Information). A TEM image of HgSe nanoparticles showed that the particles were small and spherical in nature with an

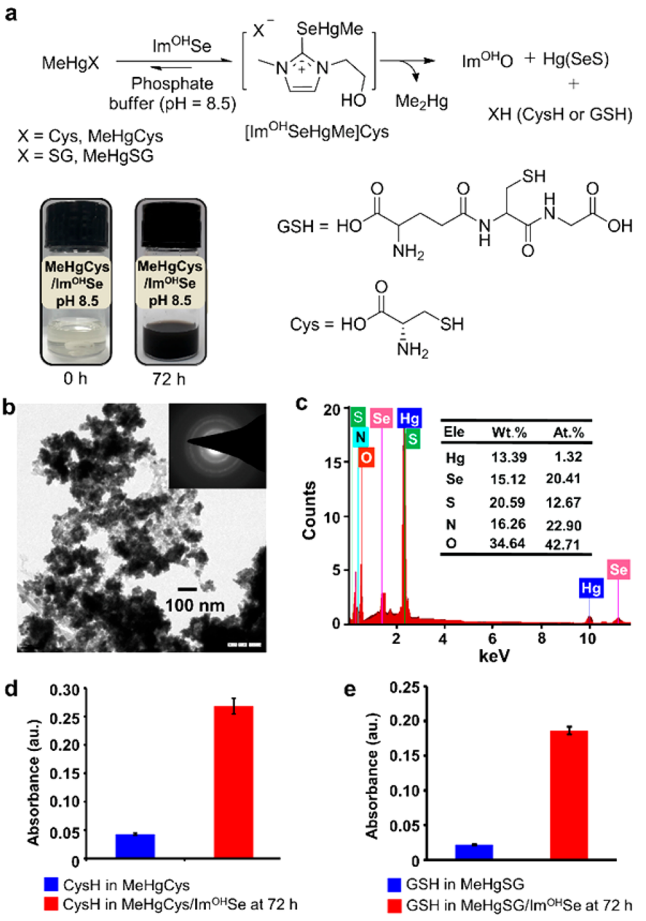


**Figure 12.** (a) Synthetic scheme for the degradation of MeHgCys or MeHgSG by $Im^{OH}Se$ and reaction vials showing the formation of Hg(SeS) NPs in the reaction of MeHgCys/$Im^{OH}Se$ in PBS buffer (pH 8.5) at 37 °C. TEM (b) and EDX (c) images of Hg(SeS) NPs obtained in the reaction of MeHgCys/$Im^{OH}Se$. Graphs showing the production of free cysteine (d) and glutathione (e) in the reaction of MeHgCys/$Im^{OH}Se$ and MeHgCys/$Im^{OH}Se$ at 72 h, respectively.

average size of 17 nm (Figure 12b). FT-IR and EDX analyses have confirmed the binding of cysteine molecules on the surface of HgSe nanoparticles (Figure S31 in the Supporting Information). EDX analysis showed the presence of both Se (atom % 20.41) and S (atom % 12.67) elements in HgSe nanoparticles. In addition, we have also detected the presence of free cysteine (8% of MeHgCys at 72 h) in the reaction solution of $Im^{OH}Se$ and MeHgCys (in 1:1 molar ratio) after 72 h of stirring at 37 °C (Figure 12d). The amounts of free cysteine present in solution were determined by Ellman's reagent (Figure S38 in the Supporting Information). These observations clearly suggest that the cysteine residues released during the reaction were distributed in two parts: few cysteine molecules remained free in the solution, and the remaining cysteine molecules attached with HgSe NPs to make water-soluble Hg(SeS) nanoparticles (Hg(SeS) hereafter)). The above reaction was also performed in water in the presence of 2 equiv of the weak base $NaHCO_3$ (the pH of the solution was found to be 8.5) and, similar to the previous case, we observed the formation of blackish gray water-soluble Hg(SeS) nanoparticles.

Likewise, we also noticed that $Im^{OH}Se$ could successfully compete with tripeptide GSH for $MeHg^+$ and convert it into water-soluble Hg(SeS) nanoparticles either in PBS buffer of pH


DOI: 10.1021/acs.inorgchem.7b01301
Inorg. Chem. XXXX, XXX, XXX−XXX

8.5 or in water plus 2 equiv of $NaHCO_3$ at 37 °C. Hg(SeS) nanoparticles obtained in the reaction of $Im^{OH}Se$ and MeHgSG were isolated and analyzed thoroughly by various techniques. TEM analysis showed that the nanoparticles were spherical in shape with an average size of 8 nm, whereas EDX and FT-IR confirmed the binding of GSH molecules on the surface of HgSe nanoparticles. The presence of free GSH was detected by LC/MS, and subsequently it was quantified by Ellman's reagent (14.5% of MeHgSG) (Figure 12e). A detailed analysis of the supernatant of the reaction solution has confirmed the formation of $Im^{OH}O$ and $Me_2Hg$ in the reaction.

In contrast, when MeHgCys or MeHgSG (30 mM) was treated with $Im^{Me}Se$ (or $Im^{OMe}Se$), which is lacking a N−$CH_2CH_2OH$ substituent, in 1:1 molar ratio in PBS buffer of pH 8.5 (or in water plus 2 equiv of $NaHCO_3$) at 37 °C, we did not observe the formation of blackish gray HgSeS nanoparticles in 72 h. These observations clearly suggest that the N−$CH_2CH_2OH$ substituent of $Im^{OH}Se$ plays a very crucial role in the cleavage of the (Im)C2−Se bond upon coordination to the mercury center of methylmercury, leading to the formation of HgSe nanoparticles and $Im^{OH}O$ in the presence of base, as shown in Schemes 1 and 3. Significantly, although the treatment of $Im^{OH}Se$ (30 mM) with MeHgCys (30 mM) in water (or PBS buffer of pH 7.0) in the absence of any base at 37 °C did not produce any blackish gray Hg(SeS) nanoparticles, we did however observe the gradual cleavage of the Hg−C bond of MeHgCys aided by $Im^{OH}Se$ under neutral conditions, as shown in Figure S37 in the Supporting Information.

In summary, we have shown that, under basic conditions (at pH 8.5), the imidazole-based selone $Im^{OH}Se$ having a N−$CH_2CH_2OH$ substituent converts MeHgCl into insoluble HgSe nanoparticles and $Me_2Hg$. However, under neutral conditions (at pH 7), $Im^{OH}Se$ facilitates the cleavage of the Hg−C bond of MeHgCl and produces $Me_2Hg$ and the cleaved product, the tetracoordinated complex $(Im^{OH}Se)_2HgCl_2$. Similarly, under basic conditions (at pH 8.5), the treatment of $Im^{OH}Se$ with MeHgCys leads to the formation of water-soluble Hg(SeS) nanoparticles, whereas at a neutral pH of 7, $Im^{OH}Se$ facilitates the cleavage of the Hg−C bond of MeHgCys. It is worth mentioning here that the presence of $Hg(S_{0.3}Se_{0.7})$ species was observed in the liver of striped dolphin (*Stenella coeruleoalba*).[20d] The formation of Hg−Se−S species in the blood of rabbits treated with a mixture of mercuric chloride and sodium selenite has also been identified.[48,49] The formation of water-soluble Hg(SeS) nanoparticles in the chemical degradation of MeHgCys or MeHgSG by benzimidazole-based selone has recently been reported by our group.[50] Significantly, we found that the imidazole-based selones $Im^{Y}Se$ have an excellent ability to demethylate both of the Hg−C bonds of highly inert $Me_2Hg$. Under acidic conditions, in the presence of excess $Im^{Me}Se$, the volatile and toxic $Me_2Hg$ degrades into $CH_4$ and the tetracoordinated mononuclear mercury compound $[(Im^{Me}Se)_4Hg]^{2+}$.

In conclusion, our experimental observations strongly suggest that the degradation of methylmercury aided by $Im^{Y}Se$ (Y = OH, OMe, Me) can be achieved at physiological temperature via two different pathways; pathway I and pathway II. Significantly, the pathway of the cleavage of Hg−C bonds of MeHgCl by $Im^{Y}Se$ is critically dependent on the nature of the N substitutent Y of $Im^{Y}Se$ and the reaction conditions. Under basic conditions, the reaction of MeHgCl with $Im^{OH}Se$ (1:1 molar ratio) afforded biologically inert HgSe and $Me_2Hg$ at physiological temperature via an efficient deselenization process assisted by the neighboring group participation of the OH group of the N−$CH_2CH_2OH$ moiety of $Im^{OH}Se$ (pathway I). On the other hand, under neutral conditions, in the absence of any base, the treatment of MeHgCl with $Im^{Y}Se$ yielded the stable cleaved products $(Im^{Y}Se)_2HgCl_2$ and $Me_2Hg$ (pathway II). Moreover, we have also shown that $Im^{OH}Se$ has a remarkable ability to convert MeHgCys or MeHgSG (cysteine or glutathione conjugated with methylmercury) to water-soluble Hg(SeS) nanoparticles via an efficient deselenization process. During this ligand exchange reaction between $Im^{OH}Se$ and MeHgCys or MeHgSG, we observed the release of free thiol CysH or GSH into the solution. However, the other selone derivatives $Im^{Me}Se$ and $Im^{OMe}Se$ that are devoid of a −$NCH_2CH_2OH$ substituent failed to convert MeHgCys or MeHgSG to Hg(SeS) nanoparticles under identical reaction conditions. Finally, we showed that, under acidic conditions, in the presence of excess $Im^{Me}Se$ the volatile and toxic $Me_2Hg$ further degraded into $[(Im^{Me}Se)_4Hg]^{2+}$.

## EXPERIMENTAL SECTION

**General Experimental Considerations.** Methylmercury chloride and ethylmercuric chloride were obtained from Alfa Aesar. Selenium powder was obtained from Sigma-Aldrich, and other chemicals were obtained from local companies. Synthetic procedures of compounds $Im^{Y}Se$ (R = OH, OMe, Me) are detailed in the Supporting Information. All experiments were carried out under anhydrous and anaerobic conditions using standard Schlenk techniques for the synthesis. Electrospray ionization high-resolution mass spectrometry (ESI-HRMS) was carried out with an Agilent 6540 accurate mass Q-TOF LC/MS (Agilent Technologies) instrument. High-performance liquid chromatography (HPLC) experiments were carried out on a Waters Alliance System (Milford, MA) consisting of an e2695 separation module and a 2998 photodiode-array detector. The HPLC system was controlled with EMPOWER software (Waters Corporation, Milford, MA). $^{1}H$ (400 MHz), $^{13}C$ (100 MHz), $^{77}Se$ (76.3 MHz), and $^{199}Hg$ (71.6 MHz) NMR spectra were obtained on a Bruker Advance 400 NMR spectrometer. Chemical shifts ($^{1}H$, $^{13}C$) are cited with respect to tetramethylsilane (TMS). $^{199}Hg$ NMR spectra are reported in ppm relative to neat $Me_2Hg$ ($\delta$ 0 ppm), and $HgCl_2$ ($\delta$ −1501 ppm for 1 M solution in DMSO-$d_6$) was used as an external standard.[32a]

**Synthetic Procedure for Tetracoordinated $HgCl_2$ Complexes of N,N-Disubstituted Selones.** *Synthesis of $(Im^{OH}Se)_2HgCl_2$.* To a solution of MeHgCl (27.6 mg, 0.11 mmol) or EtHgCl (30.2 mg, 0.11 mmol) in 4 mL of water/acetonitrile (1/1) was added 1 equiv of $Im^{OH}Se$ (22.5 mg, 0.11 mmol), and the reaction mixture was stirred at room temperature (23 °C) for 7 days to obtain a brown precipitate of $(Im^{OH}Se)_2Cl_2$, which was isolated by filtration and washed with acetonitrile (2 × 5 mL) followed by hexane (2 × 5 mL). Yield: 43 mg (53%). $^{1}H$ NMR of $(Im^{OH}Se)_2Cl_2$ (DMSO-$d_6$): $\delta$ (ppm) 3.71 (m, 10H), 4.22 (t, $J$ = 5.60 Hz, 4H), 4.45 (bs, 2H), 7.61−7.65 (m, 4H). $^{13}C$ NMR (DMSO-$d_6$): $\delta$ (ppm) 37.8, 52.9, 59.6, 123.5, 123.7, 141.3, 141.5. $^{77}Se$ NMR (DMSO-$d_6$): $\delta$ (ppm) −39. $^{199}Hg$ NMR (DMSO-$d_6$): $\delta$ (ppm) −1165. HR-ESIMS ($m/z$): calcd for $[M - Cl]^+$ $C_{12}H_{20}HgN_4O_2Se_2Cl_2$ 646.9300, found 646.9327.

*Synthesis of $(Im^{OMe}Se)_2HgCl_2$.* Compound $(Im^{OMe}Se)_2HgCl_2$ was obtained as a white crystalline material by following a procedure similar to that for $(Im^{OH}Se)_2HgCl_2$, except $Im^{OMe}Se$ (24 mg, 0.11 mmol) was added in place of $Im^{OH}Se$. Yield: 30 mg (37%). $^{1}H$ NMR of $(Im^{OMe}Se)_2HgCl_2$ (DMSO-$d_6$): $\delta$ (ppm) 3.25 (s, 6H), 3.69 (t, $J$ = 5.6 Hz, 4H), 3.77 (s, 6H), 4.34 (t, $J$ = 5.6 Hz, 4H), 7.617 (d, $J$ = 2 Hz, 2H), 7.66 (d, $J$ = 2.4 Hz, 2H), $^{13}C$ NMR (DMSO-$d_6$): $\delta$ (ppm) 37.8, 50.0, 58.6, 69.9, 123.4, 141.7. $^{77}Se$ NMR (DMSO-$d_6$): $\delta$ (ppm) −40. $^{199}Hg$ NMR (DMSO-$d_6$): $\delta$ (ppm) −1236. HR-ESIMS ($m/z$): calcd for $[M - Cl]^+$ $C_{14}H_{24}HgN_4O_2Se_2Cl_2$ 674.9614, found 674.9618.



DOI: 10.1021/acs.inorgchem.7b01301
Inorg. Chem. XXXX, XXX, XXX−XXX

*Synthesis of $(Im^{Me}Se)_2HgCl_2$.* Compound $(Im^{Me}Se)_2HgCl_2$ was obtained as a white crystalline material by following a procedure similar to that of $(Im^{OH}Se)_2HgCl_2$, except $Im^{Me}Se$ (19 mg, 0.11 mmol) was added in place of $Im^{OH}Se$. Yield: ∼26 mg (29%). $^1H$ NMR of $(Im^{Me}Se)_2HgCl_2$ (DMSO-$d_6$): $\delta$ (ppm) 3.77 (s, 6H), 7.67 (s, 2H), $^{13}C$ NMR (DMSO-$d_6$): $\delta$ (ppm) 38.0, 124.0, 140.5. $^{77}Se$ NMR (DMSO-$d_6$): $\delta$ (ppm) −40. $^{199}Hg$ NMR (DMSO-$d_6$): $\delta$ (ppm) −1229. HR-ESIMS ($m/z$): calcd for $[M - Cl]^+$ $C_{10}H_{16}HgN_4Se_2Cl_2$ 586.9088, found 586.9123.

*Synthesis of $[(Im^{Me}Se)_4Hg](BF_4)_2$.* To a solution of $Me_2Hg$ (50 mM) in DMSO-$d_6$ were added 1 equiv of tetrafluoroboric acid (45% in water) and 4 equiv of $Im^{Me}Se$ (21.1 mg, 0.12 mmol) in an NMR tube at room temperature (23 °C). The NMR tube was placed in a shaker for continuous gentle shaking for another 10 days, and then it was kept in the dark without shaking for crystallization. Cubic-shaped colorless single crystals were obtained after long standing, and the structure was analyzed by X-ray crystallography. Yield: 11 mg, 9%. $^1H$ NMR (DMSO-$d_6$): $\delta$ (ppm) 4.06 (s, 1H), 7.47 (s, 1H). $^{13}C$ NMR (DMSO-$d_6$): $\delta$ (ppm) 37.6, 123.5, 142.8. $^{77}Se$ NMR (DMSO-$d_6$): $\delta$ (ppm) −32. $^{199}Hg$ NMR (DMSO-$d_6$): $\delta$ (ppm) −1045.

**Procedure of Kinetic Studies for the Cleavage of Hg−C Bonds by $Im^YSe$ (Y = OH, OMe, Me).** We have determined the cleavage of Hg−C bonds of RHgCl (R = Me, Et) by $^1H$ NMR spectroscopy by following the procedure described below. To a solution of RHgCl (50 mM) in $CDCl_3$ was added 1 equiv of $Im^YSe$ in an NMR tube at room temperature (23 °C), and the reaction was monitored at various time intervals by $^1H$ NMR spectroscopy. Mesitylene (12 mM) was used as an external standard. In order to find out the rates of cleavage of Hg−C bonds of RHgX, the integral value of the aromatic singlet resonance of mesitylene was considered as one proton. The integral values of the singlet resonance of $MeHg^+$ ($-CH_3$) and the triplet resonance of the methyl group ($-CH_3$) of EtHgCl with respect to the aromatic singlet resonance of mesitylene were considered for the calculation of rates. The integral values at 0 min were assumed as 100% RHgCl (50 mM). All reactions were performed at least three times, and the rates are expressed as means ± standard deviation.

**Procedure for the Kinetic Studies for Decomposition of $Me_2Hg$ in the Presence or Absence of $Im^YSe$ (Y = OH, OMe, Me), under Acidic Conditions.** We have determined the cleavage of Hg−C bonds of $Me_2Hg$ under acidic conditions by $^1H$ NMR spectroscopy by following the procedure mentioned below. Briefly, to a solution of $Me_2Hg$ (50 mM) in DMSO-$d_6$ were added 1 equiv of formic acid (50% in water) and 4 equiv of $Im^{OH}Se$ (24.7 mg, 0.12 mmol) in an NMR tube at room temperature (23 °C). the NMR tube was kept in a shaker for continuous gentle shaking, and the reaction was monitored at various time intervals by $^1H$ NMR spectroscopy. In order to find out the rate of demethylation of $Me_2Hg$, we used mesitylene (12 mM) as an external standard. The integral value of the aromatic singlet resonance of mesitylene was considered as 1, and the integral value of the singlet resonance of $Me_2Hg$ ($-CH_3$) with respect to mesitylene was considered for the calculation of rates. The integral value at 0 min was assumed as 100% $Me_2Hg$ (0.05 M). All reactions were performed at least three times, and the rates are expressed as means ± standard deviation.

**General Procedure for the Degradation of MeHgCys by $Im^{OH}Se$.** $Im^{OH}Se$ (37.5 mg, 180 $\mu$mol) was added to a solution of MeHgCys (90 $\mu$mol) in 3 mL of PBS buffer (pH 8.5), and the reaction mixture was stirred at 37 °C. The clear solution gradually turned black after 4 h. After completion of the reaction (72 h), the black Hg(SeS) was isolated by centrifugation and washed thoroughly with water followed by acetonitrile. Hg(SeS) powder was dried completely under vacuum and characterized thoroughly by various techniques such as SEM, TEM, EDX, and IR analysis. For SEM and TEM analysis of Hg(SeS) NPs, 10 mg of the isolated sample was sonicated for 1 h in 10 mL of HPLC grade acetone. A 20 $\mu$L portion of a dilute solution of the sample was placed on a Cu grid and dried under vacuum and used for TEM analysis. On the other hand, 50 $\mu$L of a dilute solution of the sample was placed on a carbon grid and dried under vacuum for SEM and EDX analysis. EDX was carried out using a Zeiss EVO 40 scanning electron microscope in conjunction with a Bruker EDX system. FT-IR analyses of Hg(SeS) NPs were recorded on a Nicolet iS5 spectrometer equipped with an iD5-ATR accessory, in the range of 4000−400 $cm^{-1}$ with a resolution of 4 $cm^{-1}$.

**General Procedure for the Degradation of MeHgSG by $Im^{OH}Se$.** $Im^{OH}Se$ (37.5 mg, 180 $\mu$mol) was added to a solution of MeHgSG (90 $\mu$mol) in 3 mL of PBS buffer (pH 8.5), and the reaction mixture was stirred at 37 °C. The clear solution gradually turned black after 6 h. After completion of the reaction, the black Hg(SeS) was isolated by centrifugation and washed thoroughly with water followed by acetonitrile. Hg(SeS) powder was dried completely under vacuum and characterized thoroughly by various techniques such as SEM, TEM, EDX, and IR analysis (common procedure is mentioned above).

**X-ray Crystal Analysis.** The crystallization techniques of compounds $(Im^{OMe}Se)_2HgCl_2$ (CCDC 1541412), $(Im^{Me}Se)_2Cl_2$ (CCDC 1541411), and $[(Im^{Me}Se)_4Hg](BF_4)_2$ (CCDC 1567515)[51] are mentioned above. Crystal structures of these compounds were determined by measuring X-ray diffraction data on a D8 Venture Bruker AXS single-crystal X-ray diffractometer equipped with a CMOS PHOTON 100 detector having monochromated microfocus sources (Mo K$\alpha$ 0.71073 Å). All of the crystal data were collected at room temperature. The structure was solved using the SHELX program implemented in APEX3.[52−55] The non-H atoms were located in successive difference Fourier syntheses and refined with anisotropic thermal parameters. All of the hydrogen atoms were placed at calculated positions and refined using a riding model with appropriate HFIX commands. The program Mercury was used for molecular packing analysis.[56] Crystal data for compounds $(Im^{OMe}Se)_2HgCl_2$, $(Im^{Me}Se)_2HgCl_2$, and $[(Im^{Me}Se)_4Hg](BF_4)_2$ are given in the Supporting Information.

**Computational Details.** All of the calculations of Table 2 and Scheme 3 were performed by using the B3LYP level of theory as implemented in the Gaussian 09 package. For structure optimization the 6-311++G(2d,p) basis set was used for all atoms except Hg. The Stuttgart−Dresden basis set (SDD) was used for Hg to treat the (scalar) relativistic effects of the heavier atom, and the SDD basis set for the Hg atom was used with the corresponding relativistic effective core potential.[57] The NBO version 3.1 program implemented in Gaussian 09 was used to perform NPA for the calculation of natural charges of $Im^YSe$ and $(Im^YSe)_2HgCl_2$.[58] The natural bond orbital (NBO) analysis was performed at the B3LYP/6-311++G(2d,p) level of theory. The optimized geometries with coordinates are given in the Supporting Information.

## ■ ASSOCIATED CONTENT

### Ⓢ Supporting Information

The Supporting Information is available free of charge on the ACS Publications website at DOI: 10.1021/acs.inorgchem.7b01301.

Synthesis procedure, $^1H$, $^{13}C$, and $^{199}Hg$ NMR spectra, HR-ESIMS data, HPLC chromatogram, DFT calculations, and optimized geometries and coordinates of the optimized structures (PDF)

### Accession Codes

CCDC 1541411−1541412 and 1567515 contain the supplementary crystallographic data for this paper. These data can be obtained free of charge via www.ccdc.cam.ac.uk/data_request/cif, or by emailing data_request@ccdc.cam.ac.uk, or by contacting The Cambridge Crystallographic Data Centre, 12 Union Road, Cambridge CB2 1EZ, UK; fax: +44 1223 336033.

## ■ AUTHOR INFORMATION


### Corresponding Author

*E-mail for G.R.: Gouriprasanna.Roy@snu.edu.in.

### ORCID

Gouriprasanna Roy: 0000-0002-0047-3575




DOI: 10.1021/acs.inorgchem.7b01301
Inorg. Chem. XXXX, XXX, XXX−XXX

### Funding

This work was supported by Shiv Nadar University (SNU) and the Science and Engineering Research Board (SERB), Department of Science and Technology, Government of India, Project Number SB/S1/IC-44/2013.

### Notes

The authors declare no competing financial interest.

## ■ ACKNOWLEDGMENTS

We are grateful to Prof. Rupamanjari Ghosh (VC, SNU) for continuous support encouragement. M.B. thanks SNU for a fellowship and Ramesh Karri (SNU) for his useful advice in NMR spectroscopy. We thank the SERB, Department of Science and Technology (DST), India, for funding (Project Number SB/S1/IC-44/2013) and the AIRF (JNU) and IGIB New Delhi for TEM and SEM facilities.

## ■ ABBREVIATIONS

TEM, transmission electron microscopy; EDX, energy-dispersive X-ray spectroscopy; SEM, scanning electron microscopy

## ■ REFERENCES

(1) (a) Clarkson, T. W.; Magos, L. The Toxicology of Mercury and Its Chemical Compounds. *Crit. Rev. Toxicol.* **2006**, *36*, 609−662. (b) Morel, F. M. M.; Kraepiel, A. M. L.; Amyot, M. The chemical cycle and bioaccumulation of mercury. *Annu. Rev. Ecol. Syst.* **1998**, *29*, 543−566. (c) Bizily, S. P.; Rugh, C. L.; Meagher, R. B. Phytodetoxification of hazardous organomercurials by genetically engineered plants. *Nat. Biotechnol.* **2000**, *18*, 213−217. (d) Clarkson, T. W. The toxicology of mercury and its compounds. In *Mercury Pollution Integration and Syntehesis*; Watras, C. J., Huckabee, J. W., Eds.; Lewis Publishers: Ann Arbor, MI, 1994; pp 631−642. (e) Syversen, T.; Kaur, P. Toxicology of mercury and its compounds. *J. Trace Elem. Med. Biol.* **2012**, *26*, 215−226.

(2) (a) EPA, U. S. EPA-FDA Joint Federal Advisory for Mercury in Fish: "What You Need to Know About Mercury in Fish and Shellfish", http://www.epa.gov/mercury/ (2014). (b) EFSA. Statement on the benefits of fish/seafood consumption compared to the risks of methylmercury in fish/seafood. *EFSA Journal* **2015**, 13.

(3) (a) Aschner, M.; Aschner, J. L. Mercury neurotoxicity: Mechanisms of blood-brain barrier transport. *Neurosci. Biobehav. Rev.* **1990**, *14*, 169−176. (b) Carvalho, C. M. L.; Chew, E. H.; Hashemy, S. I.; Lu, J.; Holmgren, A. Inhibition of the Human Thioredoxin System A MOLECULAR MECHANISM OF MERCURY TOXICITY. *J. Biol. Chem.* **2008**, *283*, 11913−11923.

(4) (a) Huang, C.-F.; Liu, S.-H.; Lin-Shiau, S.-Y. Neurotoxicological effects of cinnabar (a Chinese mineral medicine, HgS) in mice. *Toxicol. Appl. Pharmacol.* **2007**, *224*, 192−201. (b) Mortimer, N. J.; Chave, T. A.; Johnston, G. A. Red tattoo reactions. *Clin. Exp. Dermatol.* **2003**, *28*, 508−510. (c) George, G. N.; Singh, S. P.; Hoover, J.; Pickering, I. J. The Chemical Forms of Mercury in Aged and Fresh Dental Amalgam Surfaces. *Chem. Res. Toxicol.* **2009**, *22*, 1761−1764. (d) Nierenberg, D. W.; Nordgren, R. E.; Chang, M. B.; Siegler, R. W.; Blayney, M. B.; Hochberg, F.; Toribara, T. Y.; Cernichiari, E.; Clarkson, T. W. Delayed Cerebellar Disease and Death after Accidental Exposure to Dimethylmercury. *N. Engl. J. Med.* **1998**, *338*, 1672−1676. (e) Korbas, M.; MacDonald, T. C.; Pickering, I. J.; George, G. N.; Krone, P. H. Chemical Form Matters: Differential Accumulation of Mercury Following Inorganic and Organic Mercury Exposures in Zebrafish Larvae. *ACS Chem. Biol.* **2012**, *7*, 411−420.

(5) (a) Harris, H. H.; Pickering, I. J.; George, G. N. The Chemical Form of Mercury in Fish. *Science* **2003**, *301*, 1203. (b) Stern, A. H.; Hudson, R. J. M.; Shade, C. W.; Ekino, S.; Ninomiya, T.; Susa, M.; Harris, H. H.; Pickering, I. J.; George, G. N. More on Mercury Content in Fish. *Science* **2004**, *303*, 763b−766.

(6) Mori, N.; Yamamoto, M.; Tsukada, E.; Yokooji, T.; Matsumura, N.; Sasaki, M.; Murakami, T. Comparison of In Vivo with In Vitro Pharmacokinetics of Mercury Between Methylmercury Chloride and Methylmercury Cysteine Using Rats and Caco2 Cells. *Arch. Environ. Contam. Toxicol.* **2012**, *63*, 628−636.

(7) (a) George, G. N.; Singh, S. P.; Prince, R. C.; Pickering, I. J. Chemical Forms of Mercury and Selenium in Fish Following Digestion with Simulated Gastric Fluid. *Chem. Res. Toxicol.* **2008**, *21*, 2106−2110. (b) Hoffmeyer, R. E.; Singh, S. P.; Doonan, C. J.; Roos, A. R. S.; Hughes, R. J.; Pickering, I. J.; George, G. N. Molecular Mimicry in Mercury Toxicology. *Chem. Res. Toxicol.* **2006**, *19*, 753−759.

(8) Roos, D. H.; Puntel, R. L.; Lugokenski, T. H.; Ineu, R. P.; Bohrer, D.; Burger, M. E.; Franco, J. L.; Farina, M.; Aschner, M.; Rocha, J. B. T.; Barbosa, N. B. de V. Complex Methylmercury−Cysteine Alters Mercury Accumulation in Different Tissues of Mice. *Basic Clin. Pharmacol. Toxicol.* **2010**, *107*, 789−792.

(9) Hirayama, K.; Yasutake, A.; Adachi, T. Mechanism for renal handling of methylmercury. In *Advances in Mercury Toxicology*; Suzuki, T., Imura, N., Clarkson, T. W., Eds.; Plenum Press: New York, 1991; pp 121−134.

(10) Yasutake, A.; Adachi, T.; Hirayama, K.; Inouye, M. Integrity of blood-brain system against methylmercury acute toxicity. *Eisei kagaku* **1991**, *37*, 355−362.

(11) Allen, J. W.; Shanker, G.; Aschner, M. Methylmercury inhibits the in vitro uptake of the glutathione precursor, cystine, in astrocytes, but not in neurons. *Brain Res.* **2001**, *894*, 131−140.

(12) (a) Hirayama, K. Transport of mechanism of methylmeruryintestinal absorption biliary excretion and distribution of methylmercury. *Kumamoto Med. J.* **1975**, *28*, 151−163. (b) Hirayama, K. Effect of amino acid on brain uptake of methylmercury. *Toxicol. Appl. Pharmacol.* **1980**, *55*, 318−23. (c) Hirayama, K. Effect of combined administration of thiol compounds and methymercury chloride on mercury distribution in rats. *Biochem. Pharmacol.* **1985**, *34*, 2030−2032.

(13) (a) Simmons-Willis, T. A.; Koh, A. S.; Clarkson, T. W.; Ballatori, N. Transport of a neurotoxicant by molecular mimicry: the methylmercury−l-cysteine complex is a substrate for human L-type large neutral amino acid transporter (LAT) 1 and LAT2. *Biochem. J.* **2002**, *367*, 239−246. (b) Yin, Z.; Jiang, H.; Syversen, T.; Rocha, J. B. T.; Farina, M.; Aschner, M. The methylmercury-L-cysteine conjugate is a substrate for the L-type large neutral amino acid transporter. *J. Neurochem.* **2008**, *107*, 1083−1090. (c) Korbas, M.; Krone, P. H.; Pickering, I. J.; George, G. N. Dynamic accumulation and redistribution of methylmercury in the lens of developing zebrafish embryos and larvae. *JBIC, J. Biol. Inorg. Chem.* **2010**, *15*, 1137−1145.

(14) (a) Kajiwara, Y.; Yasutake, A.; Adachi, T.; Hirayama, K. Methylmercury transport across the placenta via neutral amino acid carrier. *Arch. Toxicol.* **1996**, *70*, 310−314. (b) Aschner, M.; Clarkson, T. W. Methyl Mercury Uptake Across Bovine Brain Capillary Endothelial Cells in Vitro: The Role of Amino Acids. *Pharmacol. Toxicol.* **1989**, *64*, 293−297. (c) Kerper, L. E.; Ballatori, N.; Clarkson, T. W. Methylmercury transport across the blood-brain barrier by an amino acid carrier. *Am. J. Physiol.* **1992**, *262*, R761−R765.

(15) Khan, M. A.; Wang, F. Mercury-selenium compounds and their toxicological significance: Toward a molecular understanding of the mercury-selenium antagonism. *Environ. Toxicol. Chem.* **2009**, *28*, 1567−1577.

(16) Wang, F.; Lemes, M.; Khan, M. A. K. In *Environmental Chemistry and Toxicology of Mercury*; Cai, Y., Liu, G., O'Driscoll, N., Eds.; Wiley: Hoboken, NJ, 2012; Chapter 16, pp 517−544.

(17) (a) Falnoga, I.; Tusek-Znidaric, M. Selenium−Mercury Interactions in Man and Animals. *Biol. Trace Elem. Res.* **2007**, *119*, 212−220. (b) Falnoga, I.; Tusek-Znidaric, M.; Stegnar, P. The Influence of Long-term Mercury Exposure on Selenium Availability in Tissues: An Evaluation of Data. *BioMetals* **2006**, *19*, 283−294.

(18) (a) George, G. N.; MacDonald, T. C.; Korbas, M.; Singh, S. P.; Myers, G. J.; Watson, G. E.; O'Donoghue, J. L.; Pickering, I. J. The chemical forms of mercury and selenium in whale skeletal muscle.



DOI: 10.1021/acs.inorgchem.7b01301
*Inorg. Chem.* XXXX, XXX, XXX−XXX

*Metallomics* **2011**, *3*, 1232−1237. (b) Nakazawa, E.; Ikemoto, T.; Hokura, A.; Terada, Y.; Kunito, T.; Tanabe, S.; Nakai, I. The presence of mercury selenide in various tissues of the striped dolphin: evidence from μ-XRF-XRD and XAFS analyses. *Metallomics* **2011**, *3*, 719−725.
(19) Gajdosechova, Z.; Lawan, M. M.; Urgast, D. S.; Raab, A.; Scheckel, K. G.; Lombi, E.; Kopittke, P. M.; Leschner, K.; Larsen, E. H.; Woods, G.; Brownlow, A.; Read, F. L.; Feldmann, J.; Krupp, E. M. *In vivo* formation of natural HgSe nanoparticles in the liver and brain of pilot whales. *Sci. Rep.* **2016**, *6*, 34361−34371.
(20) (a) Gajdosechova, Z.; Brownlow, A.; Cottin, N. T.; Fernandes, M.; Read, F. L.; Urgast, D. S.; Raab, A.; Feldmann, J.; Krupp, E. M. Possible link between Hg and Cd accumulation in the brain of long-finned pilot whales (Globicephala melas). *Sci. Total Environ.* **2016**, *545*−*546*, 407−413. (b) Nigro, M.; Leonzio, C. Intracellular storage of mercury and selenium in different marine vertebrates. *Mar. Ecol.: Prog. Ser.* **1996**, *135*, 137−143. (c) Magos, L.; Clarkson, T. W.; Hudson, A. R. Differences in the effects of selenite and biological selenium on the chemical form and distribution of mercury after the simultaneous administration of $HgCl_2$ and selenium to rats. *J. Pharmacol. Expt. Ther.* **1984**, *228*, 478−483. (d) Ng, P.-S.; Matsumoto, K.; Yamazaki, S.; Kogure, T.; Tagai, T.; Nagasawa, H. Striped dolphin detoxificates mercury as insoluble Hg(S, Se) in the liver. *Proc. Jpn. Acad., Ser. B* **2001**, *77*, 178−183. (e) Kosta, L.; Byrne, A. R.; Zelenko, V. Correlation between selenium and mercury in man following exposure to inorganic mercury. *Nature* **1975**, *254*, 238−239. (f) Ropero, M. J. P.; Fariñas, R.; Krupp, E.; Mateo, R.; Nevado, J. J. B.; Martín-Doimeadios, R. C. R. Mercury and selenium binding biomolecules in terrestrial mammals (Cervus elaphus and Sus scrofa) from a mercury exposed area. *J. Chromatogr. B: Anal. Technol. Biomed. Life Sci.* **2016**, *1022*, 159−166.
(21) Korbas, M.; Donoghue, J. L. O.; Watson, G. E.; Pickering, I. J.; Singh, S. P.; Myers, G. J.; Clarkson, T. W.; George, G. N. The Chemical Nature of Mercury in Human Brain. *ACS Chem. Neurosci.* **2010**, *1*, 810−818.
(22) (a) Sasakura, C.; Suzuki, K. T. Biological interaction between transition metals (Ag, Cd and Hg), selenide/sulfide and selenoprotein P. *J. Inorg. Biochem.* **1998**, *71*, 159−162. (b) Suzuki, K. T.; Sasakura, C.; Yoneda, S. Binding sites for the (Hg-Se) complex on selenoprotein P. *Biochim. Biophys. Acta, Protein Struct. Mol. Enzymol.* **1998**, *1429*, 102−112. (c) Yoneda, S.; Suzuki, K. T. Detoxification of Mercury by Selenium by Binding of Equimolar Hg−Se Complex to a Specific Plasma Protein. *Toxicol. Appl. Pharmacol.* **1997**, *143*, 274−280. (d) Yoneda, S.; Suzuki, K. T. Equimolar Hg-Se Complex Binds to Selenoprotein P. *Biochem. Biophys. Res. Commun.* **1997**, *231*, 7−11. (e) Chen, C.; Yu, H.; Zhao, J.; Li, B.; Qu, L.; Liu, S.; Zhang, P.; Chai, Z. The Roles of Serum Selenium and Selenoproteins on Mercury Toxicity in Environmental and Occupational Exposure. *Environ. Health Perspect.* **2006**, *114*, 297−301.
(23) Khan, M. A. K.; Asaduzzaman, A. M.; Schreckenbach, G.; Wang, F. Synthesis, characterization and structures of methylmercury complexes with selenoamino acids. *Dalton Trans.* **2009**, 5766−5772.
(24) Khan, M. A.; Wang, F. Chemical Demethylation of Methylmercury by Selenoamino Acids. *Chem. Res. Toxicol.* **2010**, *23*, 1202−1206.
(25) Yamashita, Y.; Yamashita, M. Identification of a Novel Selenium-containing Compound, Selenoneine, as the Predominant Chemical Form of Organic Selenium in the Blood of Bluefin Tuna. *J. Biol. Chem.* **2010**, *285*, 18134−18138.
(26) Klein, M.; Ouerdane, L.; Bueno, M.; Pannier, F. Identification in human urine and blood of a novel selenium metabolite, Se-methylselenoneine, a potential biomarker of metabolization in mammals of the naturally occurring selenoneine, by HPLC coupled to electrospray hybrid linear ion trap-orbital ion trap MS. *Metallomics* **2011**, *3*, 513−520.
(27) (a) Yamashita, M.; Yamashita, Y.; Suzuki, T.; Kani, Y.; Mizusawa, N.; Imamura, S.; Takemoto, K.; Hara, T.; Hossain, A.; Yabu, T.; Touhata, K. Selenoneine, a Novel Selenium-Containing Compound, Mediates Detoxification Mechanisms against Methylmercury Accumulation and Toxicity in Zebrafish Embryo. *Mar. Biotechnol.* **2013**, *15*, 559−570. (b) Yamashita, Y.; Yamashita, Y.; Ando, T.; Wakamiya, J.; Akiba, S. Identification and Determination of Selenoneine, 2-Selenyl-Nα, Nα, Nα-Trimethyl-l-Histidine, as the Major Organic Selenium in Blood Cells in a Fish-Eating Population on Remote Japanese Islands. *Biol. Trace Elem. Res.* **2013**, *156*, 36−44.
(28) Yamashita, M.; Yamashita, Y. Selenoneine in marine organisms. In *Springer Handbook of Marine Biotechnology*; Kim, S.-K., Ed.; Springer Berlin Heidelberg: Berlin, Heidelberg, 2015; pp 1059−1069.
(29) Palmer, J. P.; Parkin, G. Protolytic Cleavage of Hg−C Bonds Induced by 1-Methyl-1,3-dihydro-2H-benzimidazole-2-selone: Synthesis and Structural Characterization of Mercury Complexes. *J. Am. Chem. Soc.* **2015**, *137*, 4503−4516.
(30) (a) Banerjee, M.; Karri, R.; Rawat, K. S.; Muthuvel, K.; Pathak, B.; Roy, G. Chemical Detoxification of Organomercurials. *Angew. Chem.* **2015**, *127*, 9455−9459; *Angew. Chem., Int. Ed.* **2015**, *54*, 9323−9327. (b) Patent App. No. PCT/IN2017/050122, 2017.
(31) (a) Roy, G.; Das, D.; Mugesh, G. Bioinorganic chemistry aspects of the inhibition of thyroid hormone biosynthesis by anti-hyperthyroid drugs. *Inorg. Chim. Acta* **2007**, *360*, 303−316. (b) Roy, G.; Jayaram, P. N.; Mugesh, G. Inhibition of Lactoperoxidase-Catalyzed Oxidation by Imidazole-Based Thiones and Selones: A Mechanistic Study. *Chem. - Asian J.* **2013**, *8*, 1910−1921.
(32) (a) Sens, M. A.; Wilson, N. K.; Ellis, P. D.; Odom, J. D. Mercury-199 fourier transform nuclear magnetic resonance spectroscopy. *J. Magn. Reson.* **1975**, *19*, 323−336. (b) Jokisaari, J.; Raisanen, K. Proton, carbon-13 and mercury-199 N.M.R. studies on dimethyl mercury in isotropic and anisotropic phases. *Mol. Phys.* **1978**, *36*, 113−123.
(33) (a) Yang, L.; Powell, R. D.; Houser, R. P. Structural variation in copper(I) complexes with pyridylmethylamide ligands: structural analysis with a new four-coordinate geometry index, $\tau_4$. *Dalton Trans.* **2007**, 955−964. (b) Okuniewski, A.; Rosiak, D.; Chojnacki, J.; Becker, B. Coordination polymers and molecular structures among complexes of mercury(II) halides with selected 1-benzoylthioureas. *Polyhedron* **2015**, *90*, 47−57.
(34) Stadelman, B. S.; Kimani, M. M.; Bayse, C. A.; McMillen, C. D.; Brumaghim, J. L. Synthesis, characterization, DFT calculations, and electrochemical comparison of novel iron (II) complexes with thione and selone ligands. *Dalton Trans.* **2016**, *45*, 4697−4711.
(35) (a) Nishio, M. The CH/π hydrogen bond in chemistry. Conformation, supramolecules, optical resolution and interactions. *Phys. Chem. Chem. Phys.* **2011**, *13*, 13873−13900. (b) Mukhopadhyay, U.; Choquesillo-Lazarte, D.; Niclos-Gutierrez, J.; Bernal, I. A critical look on the nature of the intra-molecular interligand pi, pi-stacking interaction in mixed-ligand copper (II) complexes of aromatic side-chain amino acidates and alpha, alpha'-diimines. *CrystEngComm* **2004**, *6*, 627−632.
(36) (a) Petrosyan, V. S.; Reutov, O. A. NMR spectra and structure of organomercury compounds. *J. Organomet. Chem.* **1974**, *76*, 123−169. (b) Dessy, R. E.; Flautt, T. J.; Jaffe, H. H.; Reynolds, G. F. Nuclear Magnetic Resonance Spectra of Some Dialkylmercury Compounds. *J. Chem. Phys.* **1959**, *30*, 1422. (c) Yurkerwich, K.; Quinlivan, P.; Rong, Y.; Parkin, G. Phenylselenolate mercury alkyl compounds, PhSeHgMe and PhSeHgEt: Molecular structures, protolytic Hg−C bond cleavage and phenylselenolate exchange. *Polyhedron* **2016**, *103*, 307−314.
(37) (a) Craig, P. J.; Barlett, P. D. The role of hydrogen sulphide in environmental transport of mercury. *Nature* **1978**, *275*, 635−637. (b) Rowland, I. R.; Davies, M. J.; Grasso, P. Volatilisation of methylmercuric chloride by hydrogen sulphide. *Nature* **1977**, *265*, 718−719. (c) Black, F. J.; Conaway, C. H.; Flegal, A. R. Stability of Dimethyl Mercury in Seawater and Its Conversion to Monomethyl Mercury. *Environ. Sci. Technol.* **2009**, *43*, 4056−4062.
(38) Pan-Hou, H. S. K.; Imura, N. Role of hydrogen sulfide in mercury resistance determined by plasmid of Clostridium cochlearium T-2. *Arch. Microbiol.* **1981**, *129*, 49−52.
(39) Baldi, F.; Pepi, M.; Filippelli, M. Methylmercury Resistance in Desulfovibrio desulfuricans Strains in Relation to Methylmercury Degradation. *Appl. Environ. Microbiol.* **1993**, *59*, 2479−2485.


DOI: 10.1021/acs.inorgchem.7b01301
*Inorg. Chem.* XXXX, XXX, XXX−XXX

(40) (a) Marvin-DiPasquale, M.; Agee, J.; Mcgowan, C.; Oremland, R. S.; Thomas, M.; Krabbenhoft, D.; Glimour, C. C. Methyl-Mercury Degradation Pathways: A Comparison among Three Mercury-Impacted Ecosystems. *Environ. Sci. Technol.* **2000**, *34*, 4908−4916. (b) Barkay, T.; Miller, S. M.; Summers, A. O. Bacterial mercury resistance from atoms to ecosystems. *FEMS Microbiol. Rev.* **2003**, *27*, 355−384.
(41) (a) Glendinning, K. J.; Macaskie, L. E.; Brown, N. L. Mercury Tolerance of Thermophilic *Bacillus* sp. and *Ureibacillus* sp *Biotechnol. Biotechnol. Lett.* **2005**, *27*, 1657−1662. (b) Essa, M.; Macaskie, L. E.; Brown, N. L. A New Method for Mercury Removal. *Biotechnol. Lett.* **2005**, *27*, 1649−1655. (c) Essa, A. M. M.; Creamer, N. J.; Brown, N. L.; Macaskie, L. E. A new approach to the remediation of heavy metal liquid wastes via off-gases produced by *Klebsiella pneumoniae* M426. *Biotechnol. Bioeng.* **2006**, *95*, 574−583. (d) Macaskie, L. E.; Creamer, N. J.; Essa, A. M. M.; Brown, N. L. A new approach for the recovery of precious metals from solution and from leachates derived from electronic scrap. *Biotechnol. Bioeng.* **2007**, *96*, 631−639.
(42) (a) Greene, F. D. Mechanism of Hypochlorite Decompositions. The Thermal Decomposition of L-(+)-2-Methyl-3-phenyl-2-butyl Hypochlorite. *J. Am. Chem. Soc.* **1959**, *81*, 2688−2691. (b) Dessy, R. E.; Kim, J. Y. The Rates of Reaction of Some Substituted Diarylmercury Compounds with Hydrogen Chloride. *J. Am. Chem. Soc.* **1960**, *82*, 686−689. (c) Nugent, W. A.; Kochi, J. K. Electrophilic substitution at saturated carbon in mercurials. Alkyl ligands as mechanistic probes in the cleavage of organometals. *J. Am. Chem. Soc.* **1976**, *98*, 5979−5988.
(43) (a) Strasdeit, H.; Döllen, A.; Saak, W.; Wilhelm, M. Intracellular Degradation of Diorganomercury Compounds by Biological Thiols − Insights from Model Reactions. *Angew. Chem., Int. Ed.* **2000**, *39*, 784−786. (b) Wilhelm, M.; Deeken, S.; Berssen, E.; Saak, W.; Lützen, A.; Koch, R.; Strasdeit, H. The First Structurally Authenticated Organomercury(1+) Thioether Complexes-Mercury-Carbon Bond Activation Related to the Mechanism of the Bacterial Enzyme Organomercurial Lyase. *Eur. J. Inorg. Chem.* **2004**, *2004*, 2301−2312.
(44) Cambridge Structural Database (Version 5.38, update Feb 2017): Groom, C. R.; Bruno, I. J.; Lightfoot, M. P.; Ward, S. C. *Acta Crystallogr., Sect. B: Struct. Sci., Cryst. Eng. Mater.* **2016**, *72*, 171−179.
(45) (a) Dessy, R. E.; Lee, Y. K. The Mechanism of the Reaction of Mercuric Halides with Dialkyl and Diarylmercury Compounds. *J. Am. Chem. Soc.* **1960**, *82*, 689−693. (b) Dessy, R. E.; Lee, Y. K.; Kim, J. Y. The Mechanism of the Reaction of Mercuric Iodide with Bis-organomercury Compounds. *J. Am. Chem. Soc.* **1961**, *83*, 1163−1167. (c) Murrell, L. L.; Brown, T. L. Organometallic exchange reactions VIII. Exchanges in mixtures of methylmercury halides and pseudohalides. *J. Organomet. Chem.* **1968**, *13*, 301−311.
(46) Pedrero Zayas, Z.; Querdane, L.; Mounicou, S.; Lobinski, R.; Monperrus, M.; Amouroux, D. Hemoglobin as a major binding protein for methylmercury in white-sided dolphin liver. *Anal. Bioanal. Chem.* **2014**, *406*, 1121−1129.
(47) (a) Mutter, J.; Naumann, J.; Guethlin, C. Comments on the Article "The Toxicology of Mercury and Its Chemical Compounds" by Clarkson and Magos (2006). *Crit. Rev. Toxicol.* **2007**, *37*, 537−549. (b) Shanker, G.; Aschner, J. N.; Syversen, T.; Aschner, M. Free radical formation in cerebral cortical astrocytes in culture induced by methylmercury. *Mol. Brain Res.* **2004**, *128*, 48−57. (c) Farina, M.; Rocha, J. B. T.; Aschner, M. Mechanisms of methylmercury-induced neurotoxicity: Evidence from experimental studies. *Life Sci.* **2011**, *89*, 555−563. (d) Farina, M.; Aschner, M.; Rocha, J. B. T. Oxidative stress in MeHg-induced neurotoxicity. *Toxicol. Appl. Pharmacol.* **2011**, *256*, 405−417.
(48) Gailer, J.; George, G. N.; Pickering, I. J.; Madden, S.; Prince, R. C.; Yu, E. Y.; Denton, M. B.; Younis, H. S.; Aposhian, H. V. Structural Basis of the Antagonism between Inorganic Mercury and Selenium in Mammals. *Chem. Res. Toxicol.* **2000**, *13*, 1135−1142.
(49) Khan, M. A. K.; Wang, F. Reversible Dissolution of Glutathione-Mediated $HgSe_xS_{1-x}$ Nanoparticles and Possible Significance in Hg−Se Antagonism. *Chem. Res. Toxicol.* **2009**, *22* (11), 1827−1832.
(50) Banerjee, M.; Karri, R.; Chalana, A.; Das, R.; Rawat, K. S.; Pathak, B.; Roy, G. Protection of Endogenous Thiols against Methylmercury with Benzimidazole-Based Thione by Unusual Ligand-Exchange Reactions. *Chem. - Eur. J.* **2017**, *23*, 5696−5707.
(51) CCDC 1541411, CCDC 1541412, and CCDC 1567515 contain the supplementary crystallographic data for this paper. These data can be obtained free of charge from The Cambridge Crystallographic Data Centre (CCDC) via www.ccdc.cam.ac.uk/data_request/cif.
(52) *APEX3, SAINT and SADABS: Software for data reduction, absorption correction and structure solution*; Bruker AXS Inc., Madison, WI, USA, 2015; http://www.brukersupport.com/.
(53) Sheldrick, G. M. *SHELXTL Version 2014/7: Programs for the determination of small and macromolecular crystal structures by single crystal X-ray and neutron diffraction*; University of Göttingen, Göttingen, Germany, 2014; http://shelx.uni-ac.gwdg.de/SHELX/index.php.
(54) Sheldrick, G. M. A short history of *SHELX*. *Acta Crystallogr., Sect. A: Found. Crystallogr.* **2008**, *64*, 112−122.
(55) Farrugia, L. J. ORTEP-3 for Windows - a version of ORTEP-III with a Graphical User Interface (GUI). *J. Appl. Crystallogr.* **1997**, *30*, 565.
(56) Macrae, C. F.; et al. Mercury CSD 2.0 - New Features for the Visualization and Investigation of Crystal Structures. *J. Appl. Crystallogr.* **2006**, *39*, 453−457.
(57) Figgen, D.; Rauhat, G.; Dolg, M.; Stoll, H. Energy-consistent pseudopotentials for group 11 and 12 atoms: adjustment to multi-configuration Dirac−Hartree−Fock data. *Chem. Phys.* **2005**, *311*, 227−244.
(58) Frisch, M. J., et al. *Gaussian 09, Revision B.01*; Gaussian Inc., Wallingford, CT, 2009. The full citation is given in the Supporting Information.


DOI: 10.1021/acs.inorgchem.7b01301
*Inorg. Chem.* XXXX, XXX, XXX−XXX